Review

Hydrodynamics of Biomimetic Marine Propulsion and Trends in Computational Simulations

M. I. Lamas [1],* and C. G. Rodriguez [2]

[1] Escola Politécnica Superior, Universidade da Coruña, 15403 Ferrol, Spain
[2] Technical Department, Norplan Engineering S.L., 15570 Naron, Spain; c.rodriguez.vidal@udc.es
*   Correspondence: isabel.lamas.galdo@udc.es

check for
updates

Abstract: The aim of the present paper is to provide the state of the works in the field of hydrodynamics and computational simulations to analyze biomimetic marine propulsors. Over the last years, many researchers postulated that some fish movements are more efficient and maneuverable than traditional rotary propellers, and the most relevant marine propulsors which mimic fishes are shown in the present work. Taking into account the complexity and cost of some experimental setups, numerical models offer an efficient, cheap, and fast alternative tool to analyze biomimetic marine propulsors. Besides, numerical models provide information that cannot be obtained using experimental techniques. Since the literature about trends in computational simulations is still scarce, this paper also recalls the hydrodynamics of the swimming modes occurring in fish and summarizes the more relevant lines of investigation of computational models.

Keywords: marine propulsion; biomimetics; CFD; fish

1. Introduction

Biomimetics, also called biomimicry or bionics, involves the imitation of nature in man-made systems. An area of biomimetics that is gaining an increasing interest is marine propulsion. Fish swimming is the result of millions of years of evolutionary optimization to develop a very efficient movement. For this reason, several fish movements inspire technology for marine propulsion. Marine propulsion is a multi-disciplinary area and involves numerous uses. Biomimetic marine propulsors are currently employed in oceanographic observation, military, underwater mine detection, surveillance, pipeline inspection, gas drilling, environmental awareness, rescue, etc. Fish have evolved to achieve different capabilities. Some fish are maneuverable, some are efficient, some are fast swimmers, etc. For engineering purposes, it is necessary to design the most appropriate swimming form depending on the application. For instance, oceanographic observation and pipeline inspection require high maneuvering. Other applications, such as excavation of sunken wreckage or gas drilling, require robustness and maneuvering in narrow spaces. Biological monitoring throughout large regions requires fast vehicles with the capability to travel long distances. In the military area, where spying and avoidance of detect are the two most important fields, noiseless and inconspicuous wakes are very important. In merchant ships, the most important parameter is efficiency in order to overcome the traditional propellers.

In 1936, a decisive paper was published by Gray [1], who initiated the interest in the hydrodynamics of fish swimming. Gray studied the movement of dolphins and postulated that these mammals can obtain high speeds and accelerations with a small muscle mass. He estimated the power required by a rigid model of a dolphin as about a sevenfold shortage in muscle mass to attain such speeds. He concluded that dolphin skin has special drag reduction properties. His research, known as Gray's paradox, inspired several works about the drag reduction capabilities of dolphins [2–9]. Gray's paradox

remained controversial for the following sixty years, mainly because it is extremely difficult to obtain reliable force measurements from live fish. In the 1990s, several investigations from Massachusetts Institute of Technology (MIT) reported that Gray´s calculations were wrong [10–13]. Gray had employed a rigid model of a dolphin, and these works showed that drag is lower for an undulating body than that corresponding to the rigid equivalent. Nevertheless, these authors agreed that fish employ techniques to reduce drag forces while swimming. Basically, these techniques are based on the utilization of the energy that exists in the eddies of an oncoming flow by repositioning the vorticities [14].

Great progress was made since the 1990s. Due to the increasing number of investigations about biomimetic marine propulsion, several reviews can be found in the literature. The first and most relevant one was developed by Sfakiotakis et al. [15] in 1999. This paper presented an overview of fish swimming modes, providing a classification and discussion about the relevance to underwater vehicle design. They analyzed the advantages, disadvantages, kinematics, and recommendable applications of several swimming modes. Although many mechanisms were developed after the publication of this paper, the work of Sfakiotakis et al. is still highly referenced due to its excellent explanation and classification of fish swimming modes for aquatic locomotion. Another review is the one of Cheng and Chahine [16], who presented the state of the art of swimming hydrodynamics and their biological relevance. Triantafyllou et al. [17] focused their review on the hydrodynamics of flapping foils and analyzed the implementation of such propulsion systems in marine propulsors. Colgate et al. [18] reviewed the control of robot fish, analyzing the main problems and solutions. Mittal et al. [19] reviewed the works in bio-hydrodynamics, from flapping foils to fin flexion mechanisms. Bandyopadhyay [20] reviewed aspects related to hydrodynamics, artificial muscle technology, and neuroscience-based control. Kato [21] reviewed the studies about kinematics, hydrodynamics, and performance of median and paired fin (MPF) locomotion in fish and biomimetic mechanical systems from the viewpoint of enhancing the propulsive and maneuvering performance of marine vehicles at low speeds. Chu et al. [22] centered on smart actuators used on biomimetic robots, particularly shape memory alloys, ionic polymer metal composites, and lead zirconate titanates. Raj and Thakur [23] discussed several design features like sensing, actuation, autonomy, waterproofing, and morphological structure. Other researchers [24–28] focused on flapping foils.

These reviews constitute a comprehensive state of the art of biomimetic marine propulsion. Nevertheless, the literature about trends in computational techniques is still scarce. According to this, this paper aims to supplement the literature providing the state of the works in the field of hydrodynamics and computational simulations to analyze biomimetic marine propulsors. After a description of fish swimming modes and biomimetic marine propulsors which mimic fishes, aspects related to computational simulations, such as hydrodynamics, non-dimensional parameters, turbulence, grid strategies, and experimental validations, are analyzed.

2. Fish Swimming Modes and Biomimetic Marine Propulsors

A comprehensive classification and description of the fish swimming modes was developed by Breder [29] in 1926 and expanded by Lindsey [30] in 1978. Basically, they differenced two propulsion modes: swimming and non-swimming locomotion. These are explained below.

2.1. Swimming Locomotion

The most common fish swimming modes are summarized in Figure 1. Basically, there are two factors to classify them: the extent to which the propulsion is undulatory or oscillatory and the body structures or fins that generate thrust. Most fish generate thrust using their body and/or caudal fin (BCF), for instance anguilliforms, caranguiforms, thunniforms, and ostraciiforms. Other fish, however, employ their median and/or paired fins (MPF) while the body remains practically rigid. Examples of MPF movement are amiiforms, gymnotiforms, rajiforms, labriforms, and tetraodontiforms. Several reviews [15–22] indicated that BCF modes, especially thunniform and, to a lesser extent,

caranguiform, are more efficient than MPF modes. Nevertheless, MPF modes are characterized by a high maneuverability in terms of fast start, short-radius turning, and other factors.
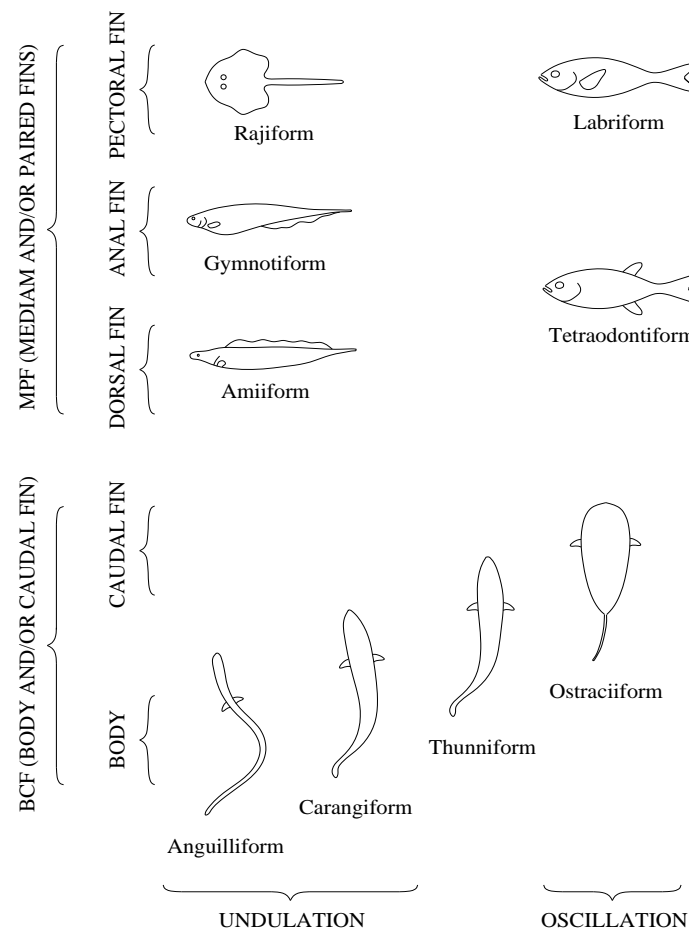

Figure 1. Examples of fish swimming modes.

The force actuating on a fish is the result of a viscous (friction) force due to the viscous shear stresses acting on the body and a pressure force due to pressure gradients. Hydrodynamically, fish locomotion can be generated by three procedures: drag-based, added mass, and momentum injection (Figure 2). Most swimmers use a combination of more than one of these procedures.
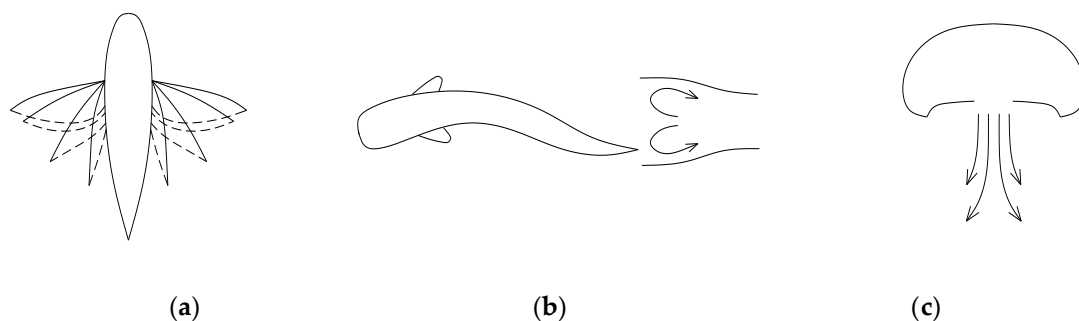

(**a**) (**b**) (**c**)

Figure 2. Main propulsion procedures from the view point of hydrodynamics; (**a**) Drag-based; (**b**) Added mass; (**c**) Momentum injection.

In the drag-based procedure (Figure 2a) a force due to the friction between the fin and water acts opposite to the direction of motion. In the added mass procedure (Figure 2b), a reaction force

is produced by the inertia of the water pushed backward by the body [31]. This propulsive force is approximately the product of the water mass accelerated and its acceleration. The momentum injection procedure (Figure 2c) is based on impulsively injecting momentum into the surrounding fluid. A force is produced by jetting fluid from the body. The momentum, which is approximately the product of the mass flow rate and the jet velocity, creates a reaction force.

Besides these locomotion procedures, most fish evolved vortex control capabilities [10–13]. This is typical of thunniform swimming mode and is presented in most fishes. As mentioned previously, dolphins have drag reduction capabilities because they employ the energy that exists in the eddies of an oncoming flow by repositioning the vortices. Despite some superficial similarities between thunniform and ostraciiform swimmers, the hydrodynamics of the latter are less efficient and based on a rigid body which achieves less vorticity control. Oscillatory movements also obtain a poorer vorticity control.

A detailed analysis of each movement and repercussion on marine propulsion is shown below.

2.1.1. BCF Swimming Modes

As indicated in Figure 1, the most common BCF swimming modes are anguilliform, caranguiform, thunniform, and ostraciiform. In anguilliform swimming mode, an undulation with constant amplitude takes place along the whole body, from head to tail. It is typical of eels, congers, muraenas, lampreys, lancelets, etc. One advantage of this movement is the turning and accelerating abilities due to the flexibility of the body. Another advantage is the possibility to swim backward, simply passing the undulation from tail to head. Due to its lower efficiency compared with other BCF modes, anguilliform swimming movement has only inspired a few robots that require high maneuverability, mimicking lampreys [32–41], snakes [42], salamanders [43–45], eels [46–51], etc.

The caranguiform mode is similar to the anguilliform one, but with the amplitude undulations growing toward the tail. Since the caranguiform swimming movement is more efficient than the anguilliform one, it inspired many more mechanisms mimicking pikes [52], salmons [53–55], sea breams [56], mackerels [57,58], etc.

As in the case of caranguiform, in thunniform swimming mode, the amplitude undulations grow toward the tail. Nevertheless, in the latter, the undulations practically take place only in the posterior half of the fish. It is typical of tunas, sharks, whales, dolphins, etc. Many researchers agree that thunniform is the most efficient swimming mode [15–22]. Among thunniform swimmers, tuna is considered the fastest fish in nature. For these reasons, most studies deal with tuna-like mechanisms [59–67]. The pioneer tuna-like mechanism was *RoboTuna* [11,59], made at MIT. This mechanism is a replica of a real tuna. Results from the *RoboTuna* project did indeed suggest a reduction in the drag force, agreeing with Gray's paradox. Following the success of the *RoboTuna* project, Anderson and Chapra at MIT improved this robot providing more vorticity control propulsion and maneuvering [60]. Another important animal that inspired thunniform mechanisms is dolphin [68–80]. The popularity of Gray's paradox made dolphins an important source of bioinspiration, and the kinematics of dolphins are among the best understood in nature. At Istanbul Technical University, Dogangil et al. also constructed a robotic dolphin [78] and analyzed the hydrodynamics and kinematics [79]. To a lesser extent, shark also inspired biomimetic propulsion mechanisms [81,82].

Ostraciiform locomotion is characterized by the pendulum-like oscillation of a rather stiff caudal fin, while the body remains essentially rigid. It is typical of cowfishes, boxfishes, coffer fishes, trunkfishes, etc. Due to its low efficiency [15,18,21], this movement has received limited attention in engineering, although an oscillating movement is easier to implement than an undulating one. Most of the investigations found in the literature are inspired by boxfish [83–86]. Other authors employed flapping foils for oscillating marine propulsors [87–101].

Table 1 summarizes the BCF swimming mechanisms mentioned, including the authors, institution, propulsion mode, and source of inspiration.

Table 1. Summary of body and/or caudal fin (BCF) swimming mechanisms.

Author	Institution	Propulsion Mode	Source of Inspiration
Cohen [32]	Cornell University, USA	Anguilliform	Lamprey
Grillner and Matsushima [33]; Grillner et al. [34]	Karolinska Institute, Sweden	Anguilliform	Lamprey
Ayers et al. [35–37]; Wilbur et al. [38]; Westphal et al. [39]	Northeastern University, USA	Anguilliform	Lamprey
Liu et al. [40]	Zhejiang University, China	Anguilliform	Lamprey
Xu et al. [41]	National University of Singapore, Singapore	Anguilliform	Eel/lamprey
Crespi et al. [42]	Swiss Federal Institute of Technology, Switzerland	Anguilliform	Sea snake
Ijspeert et al. [43]; Ijspeert et al. [44]; Crespi et al. [45]	Swiss Federal Institute of Technology, Switzerland	Anguilliform	Salamander
McIsaac and Ostrowski [46–48]	University of Western Ontario, Canada	Anguilliform	Eel
Lamas et al. [49–51]	University of A Coruña, Spain	Anguilliform	Eel
Kumph [52]	Massachussets Institute of Technology, USA	Caranguiform	Pike
Watts et al. [53–55]	University of Glasgow, United Kingdom	Caranguiform	Salmon
Hirata et al. [56]	Ship Research Institute Shinkawa, Japan	Caranguiform	Sea bream
Heo et al. [57]	Konkuk University, Korea	Caranguiform	Mackerel
Li et al. [58]	Beihang University, China	Hybrid	Mackerel
Barrett [11]; Barrett et al. [59]; Anderson and Chabra [60]	Massachussets Institute of Technology, USA	Thunniform	Tuna
Liang et al. [61]; Liang et al. [62]; Liang et al. [63]; Wang et al. [64]; Liu et al. [65]	Beihang University, China	Thunniform	Tuna
Suleman and Crawford [66]	University of Victoria, Canada	Thunniform	Tuna
Kruusmaa et al. [67]	Tallinn University of Technology, Estonia	Thunniform	Tuna
Nakashima et al. [68]; Nakashima et al. [69]; Nakashima et al. [70]; Nakashima et al. [71]	Tokyo Institute of Technology, Japan	Thunniform	Dolphin
Yu et al. [72]; Yu et al. [73]; Yu et al. [74]; Shen et al. [75]; Shen et al. [76]; Liu et al. [77]	Chinese Academy of Sciences, China	Thunniform	Dolphin
Dogangil et al. [78]; Dogangil et al. [79]	Istanbul Technical University, Turkey	Thunniform	Dolphin
Ho and Lee [80]	Konkuk University, South Korea	Thunniform	Dolphin
Aghbali et al. [81]	College of Engineering, Iran	Thunniform	Shark
Long et al. [82]	Vassar College, USA	Thunniform	Shark
Kodati et al. [83]; Kodati et al. [84]	University of Delaware, USA	Ostraciiform	Boxfish
Gordon et al. [85]	University of California, USA	Ostraciiform	Boxfish
Hu et al. [86]	Peking University, China	Ostraciiform	Boxfish
Anderson et al. [87]	Massachussets Institute of Technology, USA	Ostraciiform	Flapping foil
Read et al. [88]	Massachussets Institute of Technology, USA	Ostraciiform	Flapping foil
Yamamoto et al. [89]	Mitsubishi Heavy Industries, Japan	Ostraciiform	Flapping foil
Streitlien and Triantafyllou [90]	City College of New York, USA	Ostraciiform	Flapping foil
Paterson and Stern [91,92]	University of Lowa, USA	Ostraciiform	Flapping foil
Karpouzian et al. [93]	Univ of Southern California, USA	Ostraciiform	Flapping foil
Yamaguchi and Bose [94]	University of Tokyo, Japan	Ostraciiform	Flapping foil
Saimek and Li [95]	University of Minnesota, USA	Ostraciiform	Flapping foil
Herr and Dennis [96]	MA Institute of Technology, USA	Ostraciiform	Flapping foil
Guo [97]	Kagawa University, Japan	Ostraciiform	Flapping foil
Belibassakis and Politis [98]; Belibassakis and Filippas [99]; Filippas et al. [100]; Koutsogiannakis et al. [101]	National Technical University of Athens, Greece	Ostraciiform	Flapping foil

2.1.2. MPF Swimming Modes

As indicated in Figure 1, the most common MPF swimming modes are rajiform, amiiform, gymnotiform, labriform, and tetraodontiform. Rajiform (rays, skates, mantas, etc.), amiiform (bowfins, etc.), and gymnotiform (electrical eels, American knifefishes, etc.) modes are based on the undulation of the pectoral, dorsal, and anal fins, respectively. Nevertheless, labriform (wrasses, angelfish, surfperches, etc.) is based on the oscillation of the pectoral fin and tetraodontiform (blowfishes, etc.) on the oscillation of both anal and dorsal fins. Speed, performance, and maneuverability are key aspects of pectoral fin locomotion which provide specific application ideas for underwater vehicle technology. MPF locomotion mode is less efficient than BCF, but more maneuverable, and it is easy to reverse thrust [15,16,18]. By controlling the movement of the fins, it is possible to obtain maneuvering forces in the full six degrees of freedom and both rowing and flapping.

Due to its low efficiency, much fewer MPF mechanisms were developed by comparison with BCF mechanisms. Both oscillatory and undulatory MPF mechanisms were developed in the literature, with a preference towards pectoral fin labriform-type swimming. Concerning oscillatory-type MPF movement, labriform swimming has received special attention inspiring mechanisms that mimics black basses [102], sea turtles [103–107], sunfishes [108,109], flapping foils [110–112], rays [113–120], knifefishes [121–128], etc. Concerning undulatory-type MPF locomotion, little interest has been showed by comparison with oscillatory MPF movement. Table 2 summarizes the MPF swimming mechanisms mentioned, including the authors, institution, propulsion mode, and source of inspiration.

Table 2. Summary of median and paired fin (MPF) swimming mechanisms.

Author	Institution	Propulsion Mode	Source of Inspiration
Kato et al. [102]	Tokai University, Japan	Labriform	Black bass
Kato et al. [103]	Tokai University, Japan	Labriform	Sea turtle
Litch et al. [104,105]	Massachussets Institute of Technology, USA	Labriform	Sea turtle
Kim et al. [106]	Seoul National University, South Korea	Labriform	Sea turtle
Salumae et al. [107]	Tallinn University of Technology, Estonia	Labriform	Sea turtle
Bozkurttas et al. [108,109]	Franklin W. Olin College of Engineering, USA	Labriform	Sunfish
Georgiades et al. [110]	McGill University, Canada	Labriform	Flapping foil
Long et al. [111]	Vassar College, USA	Labriform	Flapping foil
Sitorus et al. [112]	Bandung Institute of Technology, Indonesia	Labriform	Flapping foil
Cai et al. [113]	Beihang University, China	Rajiform	Ray
Punning et al. [114]	Tartu Univeristy, Estonia	Rajiform	Ray
Chen et al. [115]	University of Virginia, USA	Rajiform	Ray
Clark and Smiths [116]	Princeton University, USA	Rajiform	Ray
Low, K.H. [117]; Zhang et al. [118,119]	Nanyang Technological University, Singapore	Rajiform	Ray
Low and Willy [120]	Nanyang Technological University, Singapore	Rajiform/gymnotiform	Ray/knifefish
Low [121]; Low [122]; Hu et al. [123]; Low [124]	Nanyang Technological University, Singapore	Gymnotiform	Knifefish
Epstein et al. [125]	Northwestern University, USA	Gymnotiform	Knifefish
McIver et al. [126,127]	Northwestern University, USA	Gymnotiform	Knifefish
Siahmansouri et al. [128]	University of Tabriz, Iran	Gymnotiform	Knifefish

In order to analyze propulsive effectiveness, most researchers use the so-called Froude efficiency. William Froude (1810–1879) was the first who used the propulsive efficiency, defined as the ratio of power output to the rate of energy input. Lamas et al. [49] developed an undulating propulsor actuated by several ribs. After that, Lamas et al. [50,51] employed CFD (Computational Fluid Dynamics) to study several amplitudes, wavelengths, and oscillation frequencies in anguilliform, carangiform, thunniform, ostraciiform, and gymnotiform movements. They concluded that thunniform is the most efficient swimming mode in terms of the Froude efficiency, followed by caranguiform, ostraciiform, anguilliform, and finally, gymnotiform. Caranguiform, ostraciiform, and anguilliform swimming modes are less efficient than thunniform because the latter produce thrust only at the tail. Nevertheless, the large undulation amplitudes along the entire body of caranguiform, anguilliform, ostraciiform, and gymnotiform swimming modes produce wasted power at the head.

It is worth mentioning that a single most appropriate swimming form does not exist. Efficiency is only one among other important assets of bioinspired aquatic propulsion such as low-speed maneuverability, fast start, and short-radius turning [129,130]. These are the most important advantages of employing a bioinspired design. Efficiency is a controversial aspect of aquatic bioinspired propulsion

since bioinspired vehicles are not merely built for their energetic efficiency, but for their suitability at dealing with tasks for which common vehicles are unfit. Fish have grown to become specialists; they excel at a range of movements their habitat and respective ecosystems dictate, but at the expense of not being well adapted to other ranges of motion. For instance, while thunniform swimming does provide superior efficiency for high cruise speed in calm water, it performs poorly at lower speeds, and provides only low levels of agility in turning maneuvers [15].

2.2. Non-Swimming Locomotion

Some aquatic animals use other mechanisms than swimming. The most important is jet propulsion (cephalopods, shellfishes, jellyfishes, etc.), based on the ejection of water behind the fish. The phenomenon is shown in Figure 3, which illustrates a vortex ring generated during contraction and another one generated during expansion. Pulsed jetting seems to have gained a growing attention in the scientific community in recent years.
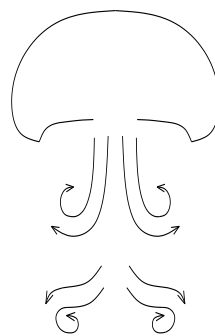

Figure 3. Schematic representation of non-swimming locomotion.

California Institute of Technology, through the works [131–136], was the first institution which studied jet propulsion. Particularly, the hydrodynamics of jet propulsion were explained in the review of Dabiri [121]. Briefly, it is based on the momentum injection procedure, i.e., water behind the fish produces a jet which generates thrust. Besides, these researchers found an important vortex optimization capability by analyzing a piston-cylinder mechanism. In their configuration, a boundary layer of vorticity forms on the inner cylinder wall as the piston moves downstream inside the cylinder, and through oscillatory jets they found that the boundary layer is less susceptible to separation; this fact mitigates turbulence. Their measurements of the impulse associated with vortex ring formation showed to be much larger than that expected from the jet velocity alone.

Table 3 summarizes the main non-swimming mechanisms, including the authors, institution, propulsion mode, and source of inspiration.

Table 3. Summary of non-swimming mechanisms.

Author	Institution	Propulsion Mode	Source of Inspiration
Gharib et al. [132]; Krueger and Gharib [133]; Krueger [134], Krueger [135], Ruiz et al. [136]	California Institute of Technology, USA	Jet	Piston-cylinder
Guo et al. [137]; Yang et al. [138]; Shi et al. [139]	Kagawa University, Japan	Jet	Jellyfish
Yeom and Oh [140]	Chonnam National University, South Korea	Jet	Jellyfish
Villanueva et al. [141]; Najem et al. [142]	Virginia Tech, USA	Jet	Jellyfish
Krieg and Mohseni [143]; Krieg and Mohseni [144]	University of Colorado, USA	Jet	Squid
Serchi et al. [145]; Serchi et al. [146]	Scuola Superiore Sant'Anna, Italy	Jet	Octopus

3. Numerical Models

3.1. Hydrodynamics

A proper design of a mechanism requires a comprehensive characterization of the fluid pattern. In this regard, numerical models can be used as an important tool to analyze the fluid flow in detail.

Between them, CFD is highly employed. This is a branch of fluid mechanics based on the split of the domain into small elements called grid or mesh. For each grid element, the governing equations are solved using numerical techniques. In a biologically inspired mechanism, the complex hydrodynamics may be computed by solution of the Navier–Stokes equations using numerical analysis. CFD provides important information that cannot be measured experimentally, such as details of the pressure field, velocity field, hydrodynamic forces, power, and efficiency. It is very useful to complement experimental works using less time and lower cost.

During the movement of the mechanism, water is pushed backward and produces a wake of alternating sign vortices known as a reverse Karman street [50,64,78,110]. This phenomenon is shown in Figure 4a,b, which represents the velocity field overlaid with the pressure field for BCF and MPF swimming modes, respectively [50]. As can be seen in these figures, several vortices are formed behind the fin. Van Buren et al. [147] manipulated the vortex structure in the wake on a pitching panel and verified important effects on thrust and efficiency. As indicated previously, it is possible to control the thrust by manipulating the flow vortex, i.e., by a mechanism of vorticity control [10,12,64]. A fish consumes much less energy to displace than a rigid body because the motion of the fish is associated with a reduction of the drag force and, thus, an increment of the propulsive efficiency by reducing separation and suppressing turbulence [148]. Recent works have shown that undulating fish movement is very efficient compared to rigid bodies [14,59,149].
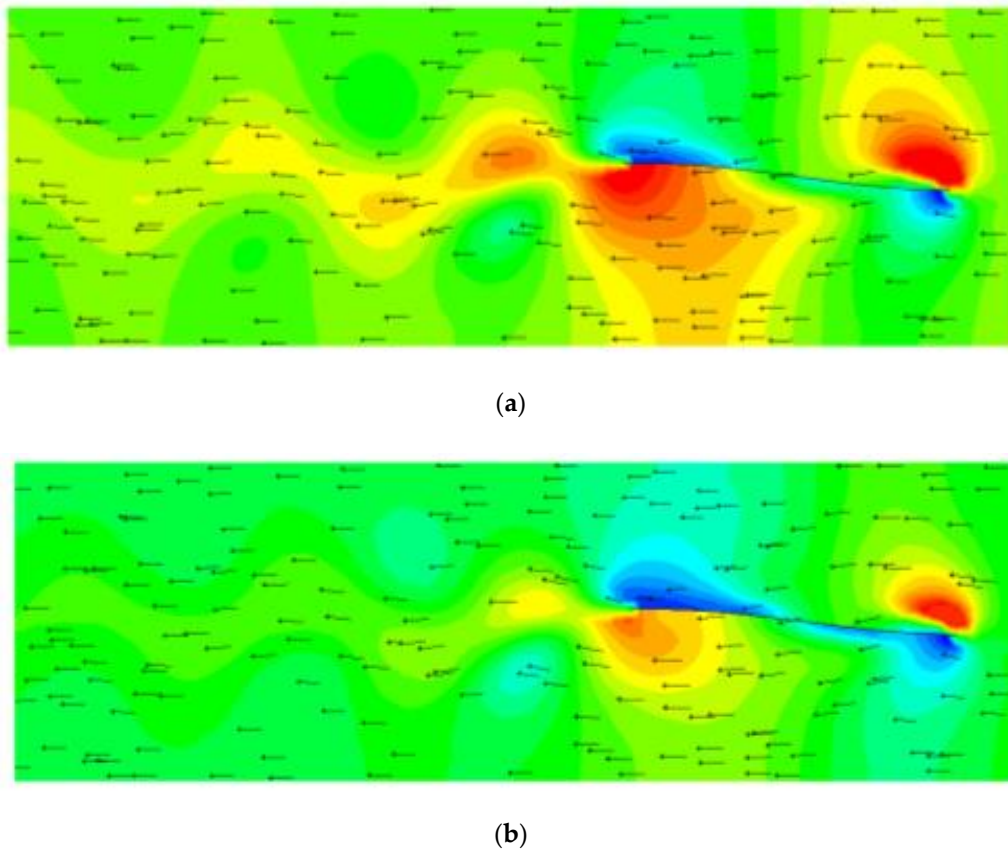
(**a**)

(**b**)

Figure 4. Velocity field overlaid with pressure field [50]; (**a**) BCF; (**b**) MPF.

The pressure differences promote a pressure force, given by:

$$\vec{F_p} = -\int_S p\hat{n}dS \qquad (1)$$

where p is the pressure, S the surface, and $\hat{n}$ a unit vector normal to the surface. On the other hand, a viscous (friction) force is produced due to the viscosity of water, and is given by the following expression:

$$\vec{F_v} = -\int_S \tau_{ij}\hat{n}dS \tag{2}$$

where τ_{ij} is the viscous stress tensor. The total force is the sum of the pressure and viscous forces. A typical distribution of the components of these forces in the direction of the movement as well as the average total force are shown in Figure 5 for anguilliform swimming mode [50]. As can be seen in this figure, the pressure and viscosity forces exhibit two peaks per cycle, corresponding to the forward and backward tail strokes. Under the conditions indicated in the figure, the propulsor accelerates since the total force is positive. If the body is accelerated, the inertia of the system contributes as an additional force, and the additional inertia of the system also promotes an added mass effect [131,150,151].
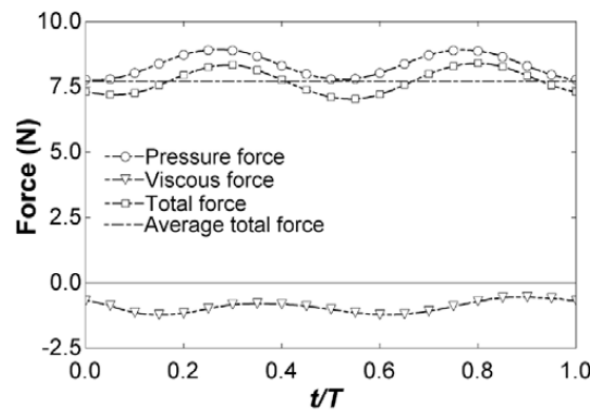

Figure 5. Time variation of the average total, total, instantaneous, and viscous forces for anguilliform swimming [50].

The average forces per cycle against the cruising velocity for anguilliform swimming are shown in Figure 6 [50]. As can be seen, when the velocity is zero, the pressure force is the maximum, and the viscous force is the minimum. As the velocity is increased, the pressure force is reduced, and the viscous force is increased until the velocity is such that the pressure force equals the viscous force, and thus, the total force is zero. Under this condition, the propulsor displaces at constant velocity, i.e., there is neither acceleration nor deceleration. In Figure 6, this velocity corresponds to 5.5 m/s. If the velocity exceeds this value, the propulsor decelerates.
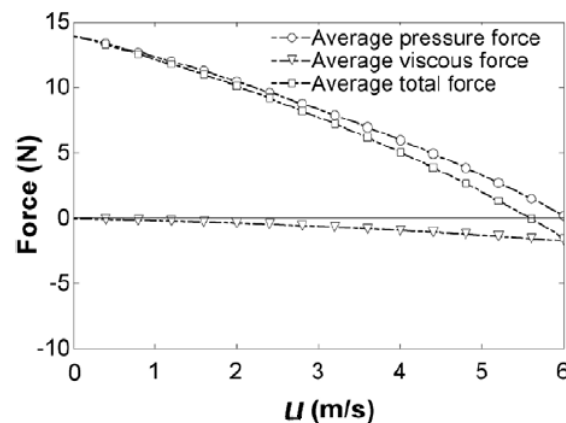

Figure 6. Average forces against cruising velocity for anguilliform swimming [50]. Reproduced or adapted from [50], with permission from Elsevier, 2020.

3.2. Non-Dimensional Parameters

In biomimetic systems, it is useful to employ non-dimensional numbers to generalize the involving parameters [49]. The governing equations corresponding to a flow around a surface are the Navier–Stokes equations of conservation of mass and momentum, given by:

$$\nabla \cdot \vec{u} = 0 \tag{3}$$

$$\frac{\partial \vec{u}}{\partial t} + \nabla \cdot (\vec{u}\vec{u}) = -\frac{\nabla p}{\rho} + \nu \nabla^2 \vec{u} + \vec{g} \tag{4}$$

where u represents the velocity, p the pressure, ρ the density, ν the kinematic viscosity, and g the gravitational acceleration. The parameters in the equations above can be converted to non-dimensional quantities by using reference values L_{ref}, u_{ref}, p_{ref}, t_{ref}, and g_{ref} for length, velocity, pressure, time, and gravitational acceleration, respectively. The non-dimensional length, velocity, pressure, time, and gravitational acceleration are given by $L^* = L/L_{ref}$, $u^* = u/u_{ref}$, $p^* = p/p_{ref}$, $t^* = t/t_{ref}$, and $g^* = g/g_{ref}$, respectively, and the resulting equations yield:

$$\frac{1}{L_{ref}}\nabla^* \cdot (\vec{u}^* u_{ref}) = 0 \tag{5}$$

$$\frac{1}{t_{ref}}\frac{\partial(\vec{u}^* u_{ref})}{\partial t^*} + \frac{1}{L_{ref}}\nabla \cdot (\vec{u}^* u_{ref}\vec{u}^* u_{ref}) = -\frac{1}{\rho}\frac{1}{L_{ref}}\nabla^*(p^* p_{ref}) + \nu \frac{1}{L_{ref}^2}\nabla^{*2}(\vec{u}^* u_{ref}) + \vec{g}^* g_{ref} \tag{6}$$

Employing the reference parameters given in Table 4, where L is the fin length and U the cruising velocity, the resulting equations of conservation of mass and momentum are given by Equations (7) and (8).

$$\frac{1}{L}\nabla^* \cdot (\vec{u}^* U) = 0 \tag{7}$$

$$\frac{U}{L}\frac{\partial(\vec{u}^* U)}{\partial t^*} + \frac{1}{L}\nabla \cdot (\vec{u}^* U\vec{u}^* U) = -\frac{1}{\rho}\frac{1}{L}\nabla^*(p^* \rho U^2) + \nu \frac{1}{L^2}\nabla^{*2}(\vec{u}^* U) + \vec{g}^* \vec{g} \tag{8}$$

which yields:

$$\nabla^* \cdot \vec{u}^* = 0 \tag{9}$$

$$\frac{\partial \vec{u}^*}{\partial t^*} + \nabla \cdot (\vec{u}^*\vec{u}^*) = -\nabla^* p^* + \frac{\nu}{UL}\nabla^{*2}\vec{u}^* + \frac{Lg}{U^2}\vec{g}^* \tag{10}$$

Table 4. Reference and non-dimensional parameters.

Dimension	Reference Parameter	Non-Dimensional Parameter
Length	$L_{ref} = L$	$L^* = L/L_{ref}$
Velocity	$u_{ref} = U$	$u^* = u/u_{ref}$
Pressure	$p_{ref} = \rho u_{ref}^2$	$p^* = p/p_{ref}$
Time	$t_{ref} = L_{ref}/u_{ref} = L/U$	$t^* = t/t_{ref}$
Gravity	$g_{ref} = g$	$\vec{g}^* = \vec{g}/g_{ref}$

Expressing the Reynolds number as $Re = UL/\nu$ and the Froude number as $Fr = U/\sqrt{Lg}$, the resulting governing equations in non-dimensional form are:

$$\nabla^* \cdot \vec{u}^* = 0 \tag{11}$$

$$\frac{\partial \vec{u}^*}{\partial t^*} + \nabla^* \cdot (\vec{u}^*\vec{u}^*) = -\nabla^* p^* + \frac{1}{Re}\nabla^{*2}\vec{u}^* + \frac{1}{Fr^2}\vec{g}^* \tag{12}$$

As can be seen, the Reynolds number, which represents the relation between inertial and viscous effects, and the Froude number, which represents the relation between inertial and gravity effects, are decisive parameters in the hydrodynamics of marine propulsors.

The frequency is usually expressed as the non-dimensional Strouhal number, *St*, given by $St = fA/U$, where *f* is the frequency and *A* the amplitude. It was highly reported that the Strouhal number is related to the vortex formation. In fact, typical values of the Strouhal number in nature are in a narrow range, approximately 0.2–0.4. Several researchers verified that the Strouhal number is related to the optimal vortex formation, which is produced in this narrow range observed in nature [59,87,149,152–155].

3.3. Turbulence

A few studies [93,156–158] employed inviscid models to analyze the hydrodynamics of biomimetic propulsion. The most important advantage of inviscid simulations is the cheap computational cost, but their accuracy is questionable. An important dimensionless parameter that involves viscosity is the Reynolds number. This parameter constitutes an indication of turbulence. The simulations that can be found in the literature span a wide range of Reynolds numbers due to the variety of values found in nature. Figure 7 shows the Reynolds number for different fish (from zebrafish larvae to stingrays and sharks), amphibians (tadpoles), reptiles (alligators), marine birds (penguins), and large mammals (from manatees and dolphins to belugas and blue whales) according to Gazzola et al. [151].
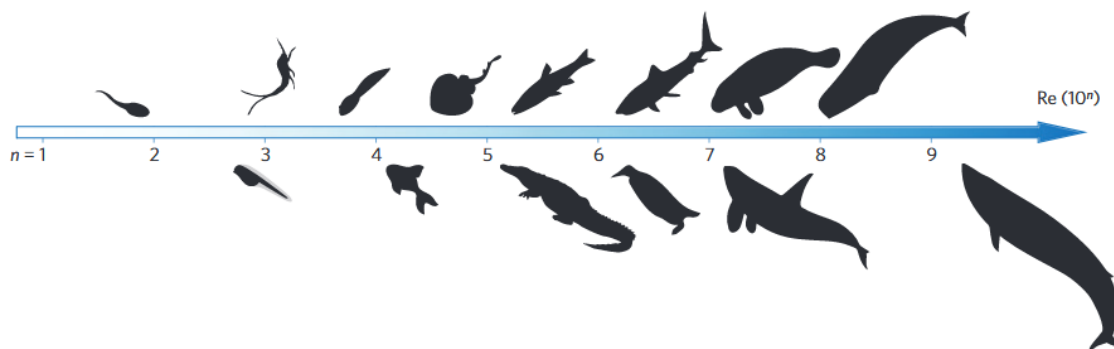

Figure 7. Reynolds number for several organisms [151]. Reproduced or adapted from [151], with permission from Elsevier, 2020.

Another important parameter is the swimming number, $Sw = fAL/\nu$. Although most numerical studies employ the Strouhal number, the swimming number provides the advantage of accounting for two length scales: amplitude and length. The swimming number is a transverse Reynolds number which characterizes the undulating movement. Gazzola et al. [152] analyzed more than 1000 measurements of fish varying in size from millimeters to meters and found that $Re \sim Sw^{\alpha}$, with $\alpha = 4/3$ for laminar flows and $\alpha = 1$ for turbulent flows. They verified that around Re 10^3–10^4, the transition from the laminar to the turbulent regime takes place, as indicated in Figure 8.

Some organisms swim at low Reynolds numbers and thus under laminar flow [149,159]. Nevertheless, most engineering biomimetic mechanisms operate at high Reynolds numbers and thus under turbulent flow. According to this, the turbulent regime was the most employed one in the numerical simulations of biomimetic propulsors.

When a body moves along a fluid, a boundary layer exists due to the "no-slip" condition and viscosity. The fluid in contact with the surface has zero velocity and, close to the surface, the fluid is slowed by frictional forces associated to the viscosity of the fluid. The result is a thin layer where the tangential velocity of the fluid increases from zero at the surface to the cruising velocity far away from the surface. The so-called boundary layer is the normal distance between the surface, where the velocity is zero, and the position where the tangential velocity is 0.95–0.99*U*, depending on the author. Flow over a wavy surface experiences adverse (flow against an increasing pressure) and favorable

pressure gradients induced by the wave motion. When a boundary layer undergoes an adverse pressure gradient, the flow near the wall decelerates. If this boundary layer has travelled far enough in the adverse pressure gradient that the velocity becomes negative, i.e., reverses the direction, separation occurs. Figure 9 shows the velocity field in the boundary layer, the last profile corresponds to reverse flow which leads to flow separation.
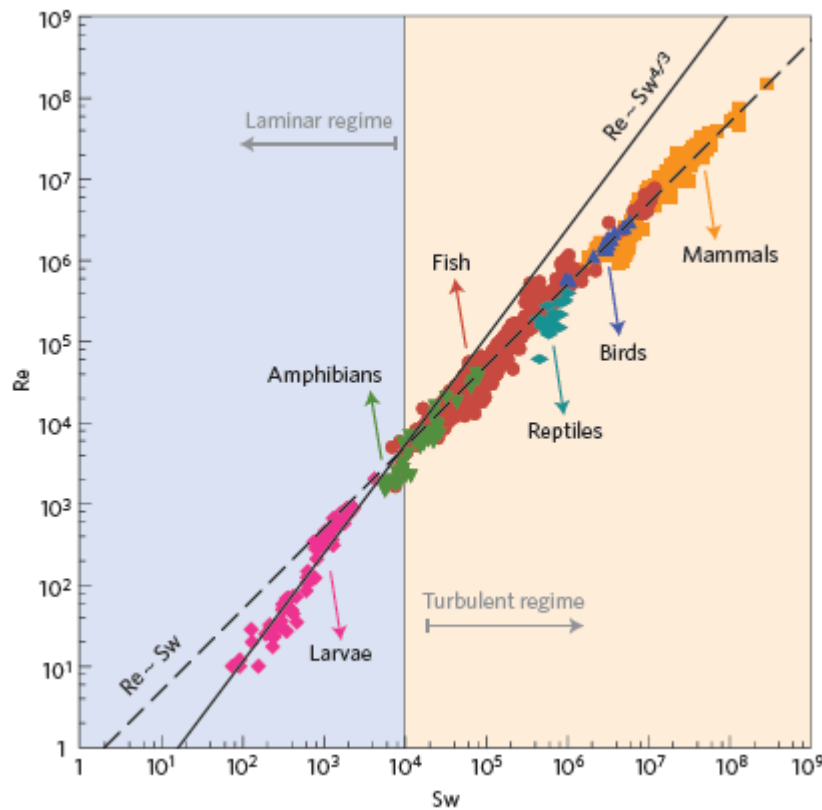

Figure 8. Reynolds against swimming number for several organisms [151].
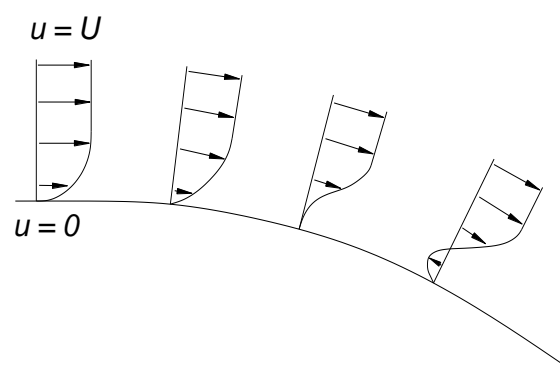
Figure 9. Velocity field at the boundary layer and flow separation (in the last profile).

Flow separation is the result of momentum losses, or decelerations, that eventually prevent the continued streamwise progress of the boundary layer fluid along the body surface. Drag is increased, and thrust is reduced. For this reason, much research has gone in the study of surfaces which delay flow separation and keep the flow attached for as long as possible. Some wave motions reduce the drag force and increase the efficiency by restraining separation and suppressing turbulence [148,160,161]. The travelling wave laminarizes the flow, and the fluid motion in the wave direction is accelerated.

The turbulence intensity is increased when separation takes place since separation is the major mechanism for turbulence production in undulating surfaces. Several authors [57,162] found that approximately when the wave phase velocity is larger than the external flow velocity, the wavy surface pushes the fluid so strongly that separation occurs.

RANS (Reynolds-averaged Navier–Stokes), LES (Large-Eddy Simulation), and DNS (Direct Numerical Simulation) approaches were employed in the literature in order to simulate turbulence. RANS procedure computes the mean flow quantities. It includes only the largest flow structures, while the smaller scales are not included. It is robust, computationally cheap, and reasonably accurate for a wide range of engineering problems. Nevertheless, the main disadvantage is that the information about the flow is limited, including the simulation of flow separation [19,163]. In biomimetic marine propulsion, the effect of separation may be important, and thus, the RANS approach does not provide an accurate prediction of the flow in the separated region. Kim et al. [164] compared six two-equation models for detachment flow and determined that the most accurate in their simulations was k-ω and k-ω_{SST} models. Another disadvantage of RANS models is the simulation of transitional laminar-turbulent flows.

Regarding DNS, this computes all the turbulent scales in the grid and temporal resolution. In DNS, the Reynolds stresses are thus not modeled. The velocity field is obtained by integrating the three-dimensional time-dependent Navier–Stokes equations. The main advantage is that this model provides accurate results, but the disadvantage is the computational cost. In the recent years, computational resources have improved noticeably and made possible several works about direct numerical simulations [165–169]. The spatial resolution required increases as the Reynolds number increases. For this reason, DNS is mostly used to study turbulent flows at low or moderate Reynolds numbers [148,168,169].

Finally, the LES approach lies between RANS and DNS. LES resolves directly large eddies, while small eddies are modeled. Resolving only the large eddies allows to use much coarser meshes and larger time-step sizes than those employed in DNS. However, LES requires substantially finer meshes than RANS. The mesh is related to the turbulence scale. The small turbulence scale becomes smaller at high Reynolds flows, and thus, it needs finer meshes, especially in the near-wall region. The high computational cost has thus become a limitation of LES for high Reynolds simulations and the main advantage is that LES provides flow separation using less computational cost than DNS [170–172].

3.4. Grid Strategies

Depending on the mathematical representation of the moving boundary, two approaches to simulate bioinspired marine propulsors can be found in the literature. The first one, known as the interface-tracking or Lagrangian method, consists in employing a moving mesh which follows the movement of the boundary. Therefore, the edges of the mesh cells are aligned to the moving boundary, as indicated in Figure 10a. The second approach, known as interface-capturing or Eulerian method, consists in employing a fixed mesh and implementing the movement of the boundary in the governing equations (Figure 10b). In this approach, the governing equations for both solid and fluid are solved simultaneously and the fluid–solid interaction in computed by source terms in the governing equations.

The habitual approach in the literature was to employ a grid that moves with the surface. Moving meshes provide accuracy but the main disadvantages are the difficulty to handle complex moving boundaries and the high computational cost. Moving meshes must be reconstructed at each time step, and the remeshing techniques increment the computational cost noticeably; in some cases, the convergence may result difficult. Fixed meshes eliminate the computational cost of remeshing procedures during the simulations. Nevertheless, the main disadvantage of fixed meshes is the accuracy. In biomimetic marine propulsion fixed meshes have been employed since the 1980s [173] and have been continued in the recent years [170–184]. These are appropriate to represent sharp movements such as free-surface boundary on the incident waves [185–188].
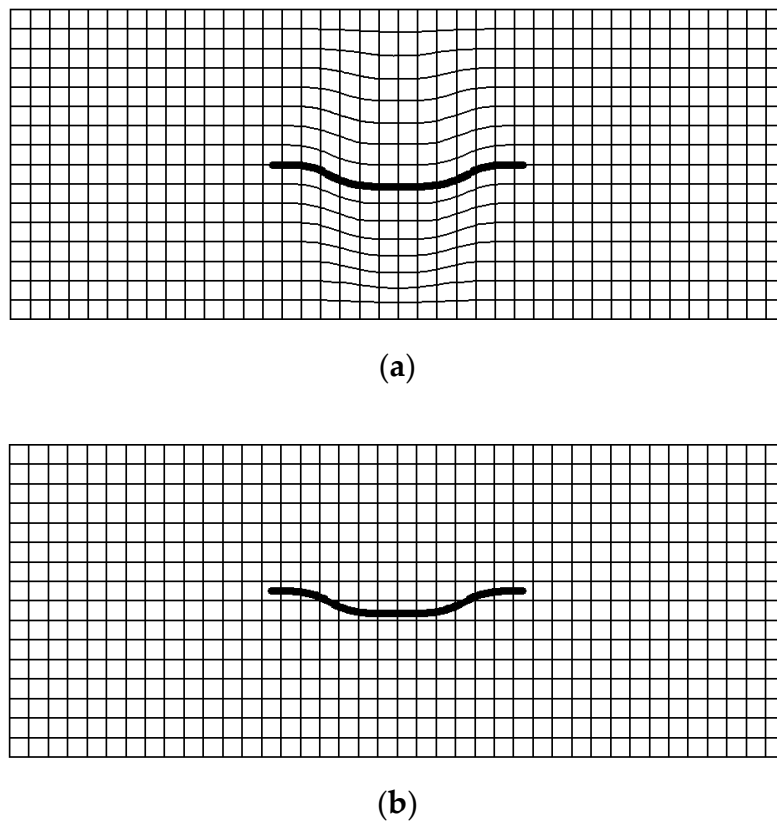
(**a**)

(**b**)

Figure 10. (**a**) Lagrangian treatment of the moving boundary; (**b**) Eulerian treatment of the moving boundary.

4. Experimental Validations

The validation process constitutes a crucial part of computational simulations. In order to validate the models and visualize the wake structures behind the propulsor, it is very common to employ PIV (Particle Image Velocimetry) [87,108,109,166,175,189,190]. This is an optical fluid measurement technique that provides instantaneous fluid velocity fields using image processing and statistics. By seeding particles in the fluid and shooting a laser sheet behind the moving surface, the flow pattern is analyzed.

During PIV, the particle concentration is such that it is possible to identify individual particles in an image, but not with certainty to track it between images. When the particle concentration is so low that it is possible to follow an individual particle, it is called PTV (Particle Tracking Velocimetry). This is a velocimetry method, i.e., a technique to measure the velocity of particles that are resident in a fluid. There are several works about PIV analysis of fishes [191–197] and robotic fishes [198,199]. Anderson et al. [200] compared PIV with PTV and found that both procedures solved the outermost regions of the boundary layer but failed to resolve the flow very close to a moving surface. In the outer regions of the boundary layer, PIV and PTV provided the same velocities; nevertheless, they recommended PTV to analyze the velocity near the surface although the errors in the results also depend on camera pixel resolution, field of view dimensions, particle shape, size, centroid analysis, and image quality. The development of high-speed digital video technology in the recent years and the availability of lower cost continuous wave lasers has facilitated these studies, and PIV and PTV are becoming a common technique among engineers and biologists. Nevertheless, these techniques must be carefully employed in order to analyze the region near the surface. An accurate determination of the velocities in this region is too important to analyze friction.

Other procedures to measure flows are LDV (Laser Doppler Velocimetry) [170], also known as LDA (Laser Doppler Anemometry), and hot-wire anemometry. The main difference between PIV and

these techniques is that the former produces two-dimensional or even three-dimensional vector fields, while the other techniques measure the velocity at a point. LDV is the technique of using the doppler shift in a laser beam to measure velocities. Buckles et al. [201] and Kuzan et al. [202] employed LDV to measure velocities working with separating flows and identified the turbulent layer and separated region. Hudson et al. [203,204] used LDV to analyze a wave surface and also analyzed the separated flow and Cherukat et al. [168] developed a computational model to analyze Hudson's results.

5. Conclusions

This work provides a state about the works in the fields of hydrodynamics and computational simulations to analyze biomimetic marine propulsion. This is an emerging field due to the advantages of biomimetic propulsion over traditional rotary propellers. The advancement of numerical methods in the recent years provides a cheap and efficient tool to analyze the hydrodynamics. The tendency of many current works is to mimic the exact shape of a real fish. One of the reasons to develop a system as a copy is the development of mechanisms capable of capturing energy from a flow. There is a great body of literature describing this phenomenon, and consequently, the hydrodynamics are now better understood. Nevertheless, numerical models provide information that cannot be obtained using experimental techniques such as details of the pressure field, velocity field, hydrodynamic forces, power, and efficiency; analyze in detail all the aspects of the problem; and isolate the effect of each parameter. The characterization of vortex formation is a complex three-dimensional problem. Given the limitations to measure these flows experimentally, numerical models constitute an important tool to characterize the vortex formation.

In the upcoming years, it is expected that the number of numerical analysis grow as computation evolve and improve some deficiencies of current works. For instance, it is very important to improve the computational resources in order to make LES and DNS more affordable. Besides, it is necessary to develop robust moving meshes algorithms which allow abrupt movements with an appropriate convergence.

In order to validate these numerical models and visualize the wake structures behind the propulsor, it is important to develop experimental works such as PIV, PTV, LDV, and other procedures. Besides, it is necessary to improve the current technology in order to obtain more precise data. Future works will focus on developing different numerical models and validate their results using experimental techniques. Once validated, these numerical models will be useful to develop new marine propulsors.

References

1. Gray, J. Studies in animal locomotion: VI. The propulsive powers of dolphin. *J. Exp. Biol.* **1936**, *13*, 192–199.
2. Gawn, R.W.L. Aspects of the locomotion of whales. *Nature* **1948**, *161*, 44–46. [CrossRef]
3. Parry, D.A. The swimming of whales and a discussion of Gray's paradox. *J. Exp. Biol.* **1949**, *26*, 24–34. [PubMed]
4. Gero, D.R. The hydrodynamic aspects of fish propulsion. *Am. Mus. Novit.* **1952**, *1601*, 1–32.
5. Kramer, M.O. Boundary layer stabilization by distributed damping. *J. Am. Soc. Nav. Eng.* **1960**, *72*, 25–33. [CrossRef]

6. Webb, P.W. *Hydrodynamics and Energetics of Fish Propulsion*; Department of the Environment Fisheries and Marine Service: Ottawa, ON, Canada, 1975; pp. 1–158.

7. Aleyev, Y.G. Hydrodynamic resistance and speed of movement of nekters. *Zool. Zhurnal* **1974**, *53*, 493–507.

8. Van Oossanen, P.; Oosterveld, M.W.C. Hydrodynamic resistance characteristics of humans, dolphins, and ship forms. *Schiffstechnik* **1989**, *36*, 31–48.

9. Fish, F.E.; Hui, C.A. Dolphin swimming—A review. *Mammal Rev.* **1991**, *21*, 181–195. [CrossRef]

10. Gopalkrishnan, R.; Triantafyllou, M.S.; Triantafyllou, G.S.; Barrett, D. Active vorticity control in a shear flow using a flapping foil. *J. Fluid Mech.* **1994**, *274*, 1–21. [CrossRef]

11. Barrett, D.S. Propulsive Efficiency of a Flexible Hull Underwater Vehicle. Ph.D. Thesis, Massachusetts Institute of Technology, Cambridge, MA, USA, 1996.

12. Anderson, J.M. Vorticity Control for Efficient Propulsion. Ph.D. Thesis, Massachusetts Institute of Technology, Cambridge, MA, USA, 1996.

13. Streitlien, K.; Triantafyllou, G.S.; Triantafyllou, M.S. Efficient foil propulsion through vortex control. *Am. Inst. Aeronaut. Astronaut. J.* **1996**, *34*, 2315–2319. [CrossRef]

14. Triantafyllou, M.S.; Triantafyllou, G.S. An efficient swimming machine. *Sci. Am.* **1995**, *272*, 64–70. [CrossRef]

15. Sfakiotakis, M.; Lane, D.M.; Davies, J.B.C. Review of fish swimming modes for aquatic locomotion. *IEEE J. Ocean. Eng.* **1999**, *24*, 237–252. [CrossRef]

16. Cheng, J.Y.; Chahine, G.L. Computational hydrodynamics of animal swimming: Boundary element method and three dimensional vortex wake structure. *Comp. Biochem. Physiol. Part A* **2001**, *131*, 51–60. [CrossRef]

17. Triantafyllou, M.S.; Techet, A.; Hover, F.S. Review of experimental work in biomimetic foils. *IEEE J. Ocean. Eng.* **2004**, *29*, 585–594. [CrossRef]

18. Colgate, J.E. Mechanics and control of swimming: A review. *IEEE J. Ocean. Eng.* **2004**, *29*, 660–673. [CrossRef]

19. Mittal, R. Computational modelling in bio-hydrodynamics: Trends, challenges and recent advances. *IEEE J. Ocean. Eng.* **2004**, *29*, 595–604. [CrossRef]

20. Bandyopadhyay, P.R. Trends in biorobotic autonomous undersea vehicles. *IEEE J. Ocean. Eng.* **2005**, *30*, 109–139. [CrossRef]

21. Kato, N. Median and paired fin controllers for biomimetic marine vehicles. *Appl. Mech. Rev.* **2005**, *58*, 238–252. [CrossRef]

22. Chu, W.S.; Lee, K.T.; Song, S.H.; Han, M.W.; Lee, J.Y.; Kim, H.S.; Kim, M.S.; Park, Y.J.; Cho, K.J.; Ahn, S.H. Review of biomimetic underwater robots using smart actuators. *Int. J. Precis. Eng. Manuf.* **2012**, *13*, 1281–1292. [CrossRef]

23. Raj, A.; Thakur, A. Fish-inspired robots: Design, sensing, actuation, and autonomy—A review of research. *Bioinspir. Biomim.* **2016**, *11*. [CrossRef]

24. Rozhdestvensky, K.; Ryzhov, V. Aerodynamics of flapping-wing propulsors. *Prog. Aerosp. Sci.* **2003**, *39*, 585–633. [CrossRef]

25. Naito, S.; Isshiki, H. Effect of bow wings on ship propulsion and motions. *Appl. Mech. Rev.* **2005**, *58*, 253–268. [CrossRef]

26. Shyy, W.; Aono, H.; Chimakurthi, S.K.; Trizilia, P.; Kang, C.K.; Cesnik, H.L.C.E.S. Recent progress in flapping wing aerodynamics and aeroelasticity. *Prog. Aerosp. Sci.* **2010**, *46*, 284–327. [CrossRef]

27. Xiao, Q.; Zhu, Q. A review on flow energy harvesters based on flapping foils. *J. Fluids Struct.* **2014**, *46*, 174–191. [CrossRef]

28. Wu, X.; Zhang, X.; Tian, X.; Li, X.; Lu, W. A review on fluid dynamics of flapping foils. *Ocean. Eng.* **2019**, *195*, 106712. [CrossRef]

29. Breder, C.M. The locomotion of fishes. *Zoologica* **1926**, *4*, 159–297.

30. Lindsey, C.C. Form, function and locomotory habits in fish. *Fish Physiol.* **1978**, *7*, 1–100. [CrossRef]

31. Metin, S.; Menciassi, A.; Low, K.H.; Kim, S. Survey and introduction to the focused section on bio-inspired mechatronics. *IEEE/ASME Trans. Mechatron.* **2013**, *18*, 409–418. [CrossRef]

32. Cohen, A.H.; Colmes, P.J.; Rand, R.H. The nature of the coupling between segmental oscillators of the lamprey spinal generator for locomotion: A mathematical model. *J. Math. Biol.* **1982**, *13*, 345–369. [CrossRef]

33. Grillner, S.; Deliagina, T.; Ekeberg, A.; Manira, R.H.; Lansner, H.A.; Orlovsky, G.N.; Wallen, P. Neural networks that coordinate locomotion and body orientation in the lamprey. *Trends Neurosci.* **1995**, *18*, 270–279. [CrossRef]

34. Grillner, S.; Matsushima, T. The neural network underlying locomotion in lamprey—Synaptic and cellular mechanisms. *Neuron* **1991**, *7*, 1–15. [CrossRef]

35. Ayers, J.; Wilbur, C.; Olcott, C. Lamprey robots. In Proceedings of the 1st International Symposium of Aqua Bio-Mechanisms, ISABMEC 2000, Tokai University Pacific Center, Honolulu, HI, USA, 27–30 August 2000.

36. Ayers, J.; Rulkov, N.; Knudsen, D.; Kim, Y.B.; Volkovskii, A.; Selverston, A. Controlling underwater robots with electronic nervous systems. *Appl. Bionics Biomech.* **2010**, *7*, 57–67. [CrossRef]

37. Ayers, J.; Westphal, A.; Blustein, D. A conserved neural circuit-based architecture for ambulatory and undulatory biomimetic robots. *Mar. Technol. Soc. J.* **2011**, *45*, 147–152. [CrossRef]

38. Wilbur, C.; Vorus, W.; Cao, Y.; Currie, S.N. A lamprey-based undulatory vehicle. In *Neurotechnology for Biomimetic Robots*; MIT Press: Cambridge, MA, USA, 2002; pp. 285–296.

39. Westphal, A.; Rulkov, N.F.; Ayers, J.; Brady, D.; Hunt, M. Controlling a lamprey-based robot with an electronic nervous system. *Smart Struct. Syst.* **2011**, *8*, 39–52. [CrossRef]

40. Liu, W.; Li, F.; Stefanini, C.; Chena, D.; Dario, P. Biomimetic flexible/compliant sensors for a soft-body lamprey-like robot. *Robot. Auton. Syst.* **2010**, *58*, 1138–1148. [CrossRef]

41. Xu, J.X.; Niu, X.L.; Ren, Q.Y. Modeling and control design of an anguilliform robotic fish. *Int. J. Model. Simul. Sci. Comput.* **2012**, *3*, 1250018. [CrossRef]

42. Crespi, A.; Badertscher, A.; Guignard, A.; Ijspeert, A.J. AmphiBot I: An amphibious snake-like robot. *Robot. Auton. Syst.* **2005**, *50*, 163–175. [CrossRef]

43. Ijspeert, J.A. A connectionist central pattern generator for the aquatic and terrestrial gaits of a simulated salamander. *Biol. Cybern.* **2001**, *84*, 331–348. [CrossRef]

44. Ijspeert, A.J.; Crespi, A.; Cabelguen, J.M. Simulation and robotics studies of salamander locomotion: Applying neurobiological principles to the control of locomotion in robots. *Neuroinformatics* **2005**, *3*, 171–195. [CrossRef]

45. Crespi, A.; Karakasiliotis, K.; Guignard, A.; Ijspeert, A.J. Salamandra Robotica II: An amphibious robot to study salamander-like swimming and walking gaits. *IEEE Trans. Robot.* **2013**, *29*, 308–320. [CrossRef]

46. McIsaac, K.P.; Ostrowski, J.P. Experiments in closed-loop control for an underwater eel-like robot. In Proceedings of the IEEE International Conference on Robotics and Automation, Washington, DC, USA, 11–15 May 2002; pp. 750–755. [CrossRef]

47. McIsaac, K.P.; Ostrowski, J.P. Experimental verification of open-loop control for an underwater eel-like robot. *Int. J. Robot. Res.* **2002**, *21*, 849–859. [CrossRef]

48. McIsaac, K.P.; Ostrowski, J.P. Motion planning for anguilliform locomotion. *IEEE Trans. Robot. Autom.* **2003**, *19*, 637–652. [CrossRef]

49. Lamas, M.I.; Rodríguez, J.D.; Rodríguez, C.G.; González, P.B. Design aspects and two-dimensional CFD simulation of a marine propulsor based on a biologically-inspired undulating movement. *J. Marit. Res.* **2020**, *7*, 73–88.

50. Lamas, M.I.; Rodríguez, J.D.; Rodríguez, C.G. CFD analysis of biologically-inspired marine propulsors. *Brodogradnja* **2012**, *63*, 125–133.

51. Lamas, M.I.; Rodríguez, J.D.; Rodríguez, C.G.; González, P.B. Three-dimensional CFD analysis to study the thrust and efficiency of a biologically-inspired marine propulsor. *Pol. Marit. Res.* **2011**, *18*, 10–16. [CrossRef]

52. Kumph, J.M. Maneuvering of a Robotic Pike. Mater's Thesis, Department of Ocean Engineering, Massachussets Institute of Technology, Cambridge, MA, USA, 2000.

53. Watts, C.M. A Comparison Study of Biologically Inspired Propulsion Systems for an Autonomous Underwater Vehicle. Ph.D. Thesis, University of Glasgow, Glasgow, UK, 2009.

54. Watts, C.; McGookin, E.; Macauley, M. Biomimetic propulsion systems for mini-autonomous underwater vehicles. In Proceedings of the IEEE Conference OCEANS 2007, Vancouver, BC, Canada, 29 September–4 October 2007. [CrossRef]

55. Watts, C.; McGookin, E. Modeling and simulation of a biomimetic underwater vehicle. In Proceedings of the Grand Challenges in Modeling and Simulation symposium, Edinburgh, UK, 16–19 June 2008; pp. 402–408.

56. Hirata, K.; Takimoto, T.; Tamura, K. Study on turning performance of a fish robot. In Proceedings of the 1st International Symposium of Aqua Bio-Mechanisms, ISABMEC 2000, Tokai University Pacific Center, Honolulu, HI, USA, 27–30 August 2000.

57. Heo, S.; Wiguna, T.; Park, H.C.; Goo, N.S. Effect of an artificial caudal fin on the performance of a biomimetic fish robot propelled by piezoelectric actuators. *J. Bionic Eng.* **2007**, *4*, 151–158. [CrossRef]

58. Li, W.; Tianmiao, W.; Guanhao, W.; Jianhong, L. Hybrid undulatory kinematics of a robotic Mackerel (Scomber scombrus): Theoretical modeling and experimental investigation. *Sci. China Technol. Sci.* **2012**, *55*, 2941–2952. [CrossRef]

59. Barrett, D.S.; Triantafyllou, M.S.; Yue, D.K.P. Drag reduction in fish-like locomotion. *J. Fluid Mech.* **1999**, *392*, 183–212. [CrossRef]

60. Anderson, J.M.; Chabra, N.K. Maneuvering and stability performance of a robotic tuna. *Integr. Comp. Biol.* **2002**, *42*, 118–126. [CrossRef]

61. Liang, J.; Wen, L.; Guo, Y. Experimental design and performance of underwater vehicle based on capacity of voyage. In Proceedings of the IEEE International Conference on Robotics, Automation and Mechatronics, Chengdu, China, 21–24 September 2008; pp. 587–591. [CrossRef]

62. Liang, J.; Zheng, W.; Wen, L.; Wang, T.; Xie, C. Propulsive and maneuvering performance of two joints biorobotic autonomous undersea vehicle. In Proceedings of the IEEE International Conference on Robotics and Biomimetics, Guilin, China, 19–23 December 2009; pp. 314–320. [CrossRef]

63. Liang, J.; Wang, T.; Wen, L. Development of a two-joint robotic fish for real-world exploration. *J. Field Robot.* **2011**, *28*, 70–79. [CrossRef]

64. Wang, T.; Wen, L.; Liang, J.; Wu, G. Fuzzy vorticity control of a biomimetic robotic fish using a flapping lunate tail. *J. Bionic Eng.* **2010**, *7*, 56–65. [CrossRef]

65. Liu, Y.X.; Chen, W.S.; Liu, J.K. Research on the swing of the body of two-joint robot fish. *J. Bionic Eng.* **2008**, *5*, 159–165. [CrossRef]

66. Suleman, A.; Crawford, C. Design and testing of a biomimetic tuna using shape memory alloy induced propulsion. *Comput. Struct.* **2008**, *86*, 491–499. [CrossRef]

67. Kruusmaa, M.; Fiorini, P.; Megill, W.; de Vittorio, M.; Akanyeti, O.; Visentin, F.; Chambers, L.; El Daou, H.; Fiazza, M.C.; Ježov, J.; et al. FILOSE for svenning: A flow sensing bioinspired robot. *IEEE Robot. Autom. Mag.* **2014**, *21*, 51–62. [CrossRef]

68. Nakashima, M.; Tokuo, K.; Kaminaga, K.; Ono, K. Experimental study of a self-propelled two-joint dolphin robot. In Proceedings of the Ninth International Offshore and Polar Engineering Conference, Brest, France, 30 May–4 June 1999.

69. Nakashima, M.; Ono, K. Development and experiment of two-joint dolphin robot. In *Neurotechnology for Biomimetic Robots*; MIT Press: Cambrige, MA, USA, 2002; pp. 309–324.

70. Nakashima, M.; Takashi, Y.; Ono, K. Three dimensional manoeuverability of the dolphin robot. In *Bio-Mechanisms of Swimming and Flying*; Springer: Tokio, Japan, 2004; pp. 79–92. [CrossRef]

71. Nakashima, M.; Tsubaki, T.; Ono, K. Three-dimensional movement in water of the dolphin robot—Control between two positions by roll and pitch combination. *J. Robot. Mechatron.* **2006**, *18*, 347–355. [CrossRef]

72. Yu, J.; Hu, Y.; Fan, R.; Wang, L.; Kuzucu, A. Mechanical design and motion control of biomimetic robotic dolphin. *Adv. Robot.* **2007**, *21*, 499–513. [CrossRef]

73. Yu, J.; Hu, Y.; Huo, J.; Wang, L. An adjustable Scotch Yoke mechanism for robotic dolphin. In Proceedings of the IEEE International Conference on Robotics and Biomimetics, Sanya, China, 15–28 December 2007; pp. 513–518. [CrossRef]

74. Yu, J.; Hu, Y.; Huo, J.; Wang, L. Dolphin-like propulsive mechanism based on an adjustable Scotch yoke. *Mech. Mach. Theory* **2009**, *44*, 603–614. [CrossRef]

75. Shen, F.; Wei, C.; Cao, Z.; Xu, D.; Yu, J.; Zhou, C. Implementation of a multi-link robotic dolphin with two 3-DOF flippers. *J. Comput. Inf. Syst.* **2011**, *7*, 2601–2607.

76. Shen, F.; Cao, Z.Q.; Xu, D.; Zhou, C. A dynamic model of robotic dolphin based on Kane method and its speed optimization method. *Acta Autom. Sin.* **2012**, *38*, 1247–1256. [CrossRef]

77. Liu, P.; He, K.; Ou, X.; Du, R. Mechanical design, kinematic modeling and simulation of a robotic dolphin. In Proceedings of the IEEE International Conference on Information and Automation, Shenzhen, China, 6–8 June 2011. [CrossRef]

78. Dogangil, G.; Ozcicek, E.; Kuzucu, A. Design, construction, and control of a robotic dolphin. In Proceedings of the IEEE International Conference on Robotics and Biomimetics, Shatin, China, 5–9 July 2005; pp. 51–56. [CrossRef]

79. Dogangil, G.; Ozcicek, E.; Kuzucu, A. Modeling, simulation, and development of a robotic dolphin prototype. In Proceedings of the IEEE International Conference on Mechatronics and Automation, Niagara Falls, ON, Canada, 29 July–1 August 2005; pp. 952–957. [CrossRef]

80. Ho, T.; Lee, S. Design of a multi-locomotion underwater robot. *Adv. Mater. Res.* **2012**, *488*, 1732–1736. [CrossRef]

81. Aghbali, B.; Yousefi-Koma, A. Design and fuzzy control of the shark robot-fish dorsal fin using SMA. In Proceedings of the 10th Biennial Conference on Engineering Systems Design and Analysis, Istanbul, Turkey, 12–14 July 2010. [CrossRef]

82. Long, J.H., Jr.; Koob, T.; Schaefer, J.; Summers, A.; Bantilan, K.; Grotmol, S.; Porter, M. Inspired by sharks: A biomimetic skeleton for the flapping, propulsive tail of an aquatic robot. *Mar. Technol. Soc. J.* **2011**, *45*, 119–129. [CrossRef]

83. Kodati, P.; Hinkle, J.; Deng, X. Micro autonomous robotic ostraciiform (MARCO): Design and fabrication. In Proceedings of the IEEE International Conference on Robotics and Automation, Rome, Italy, 14–15 April 2007. [CrossRef]

84. Kodati, P.; Hinkle, J.; Winn, A.; Deng, X. Microautonomous robotic ostraciiform (MARCO): Hydrodynamics, design, and fabrication. *IEEE Trans. Robot.* **2008**, *24*, 105–111. [CrossRef]

85. Gordon, M.; Hove, J.; Webb, P.; Weihs, D. Boxfishes as unusually well-controlled autonomous underwater vehicles. *Physiol. Biochem. Zool.* **2000**, *74*, 663–671. [CrossRef] [PubMed]

86. Hu, Y.; Zhao, W.; Xie, G.; Wang, L. Development and target following of vision-based autonomous robotic fish. *Robotica* **2009**, *27*, 1075–1089. [CrossRef]

87. Anderson, J.M.; Streitlien, K.; Barrett, D.S.; Triantafyllou, M.S. Oscillating foils of high propulsive efficiency. *J. Fluid Mech.* **1998**, *360*, 41–72. [CrossRef]

88. Read, D.A.; Hover, F.S.; Triantafyllou, M.S. Forces on oscillating foils for propulsion and maneuvering. *J. Fluids Struct.* **2003**, *17*, 163–183. [CrossRef]

89. Yamamoto, I.; Terada, Y.; Nagamatu, T.; Imaizumi, Y. Propulsion system with flexible/rigid oscillating fin. *IEEE J. Ocean. Eng.* **1995**, *20*. [CrossRef]

90. Streitlien, K.; Triantafyllou, G.S. On thrust estimates for flapping foils. *J. Fluids Struct.* **1998**, *12*, 47–55. [CrossRef]

91. Paterson, E.G.; Stern, F. Computation of unsteady viscous marine-propulsor blade flows—Part 1: Validation and analysis. *J. Fluids Eng. Trans. ASME* **1997**, *119*, 145–154. [CrossRef]

92. Paterson, E.G.; Stern, F. Computation of unsteady viscous marine-propulsor blade flows—Part 2: Parametric study. *J. Fluids Eng. Trans. ASME* **1999**, *121*, 139–147. [CrossRef]

93. Karpouzian, G.; Spedding, G.; Cheng, H.K. Lunate-tail swimming propulsion. Part 2. Performance analysis. *J. Fluid Mech.* **1990**, *210*, 329–351. [CrossRef]

94. Yamaguchi, H.; Bose, N. Oscillating foils for marine propulsion. In Proceedings of the 4th International Offshore and Polar Engineering Conference, Osaka, Japan, 10–15 April 1994; Volume 3, pp. 539–544.

95. Saimek, S.; Li, P.Y. Motion planning and control of a swimming machine. In Proceedings of the American Control Conference, Arlington, VA, USA, 25–27 June 2001; pp. 125–130. [CrossRef]

96. Herr, H.; Dennis, B. A swimming robot actuated by living muscle tissue. *J. Neuroeng. Rehabil.* **2004**, *1*, 6–9. [CrossRef]

97. Guo, S. A new type of fish-like underwater microrobot. *IEEE/ASME Trans. Mechatron.* **2003**, *8*, 136–141. [CrossRef]

98. Belibassakis, K.A.; Politis, G.K. Hydrodynamic performance of flapping wings for augmenting ship propulsion in waves. *Ocean. Eng.* **2013**, *72*, 227–240. [CrossRef]

99. Belibassakis, K.A.; Filippas, E.S. Ship propulsion in waves by actively controlled flapping foils. *Appl. Ocean. Res.* **2015**, *52*, 1–11. [CrossRef]

100. Filippas, E.; Gerostathis, G.; Belibassakis, K.A. Semi-activated oscillating hydrofoil as a nearshore biomimetic energy device system in waves and currents. *Ocean. Eng.* **2018**, *154*, 396–415. [CrossRef]

101. Koutsogiannakis, P.E.; Filippas, E.S.; Belibassakis, K.A. A study of multi-component oscillating-foil hydrokinetic turbines with a GPU-accelerated boundary element method. *J. Mar. Sci. Eng.* **2019**, *7*, 424. [CrossRef]

102. Kato, N. Control performance in the horizontal plane of a fish robot with mechanical pectoral fins. *IEEE J. Ocean. Eng.* **2000**, *25*, 121–129. [CrossRef]

103. Kato, N. Swimming and walking of an amphibious robot with fin actuators. *Mar. Technol. Soc. J.* **2011**, *45*, 181–197. [CrossRef]

104. Licht, S.; Polidoro, V.; Flores, M.; Hover, F.S.; Triantafyllou, M.S. Design and projected performance of a flapping foil AUV. *IEEE J. Ocean. Eng.* **2004**, *29*, 786–794. [CrossRef]

105. Licht, S.C.; Wibawa, M.S.; Hover, F.S.; Triantafyllou, M.S. In-line motion causes high thrust and efficiency in flapping foils that use power downstroke. *J. Exp. Biol.* **2010**, *213*, 63–71. [CrossRef] [PubMed]

106. Kim, H.J.; Song, S.H.; Ahn, S.H. A turtle-like swimming robot using a smart soft composite (SSC) structure. *Smart Mater. Struct.* **2013**, *22*, 014007. [CrossRef]

107. Salumae, T.; Raag, R.; Rebane, J.; Ernits, A.; Toming, G.; Ratas, M.; Kruusmaa, M. Design principle of a biomimetic underwater robot U-CAT. In Proceedings of the 2014 Oceans, St. John's, NL, Canada, 14–19 September 2014; pp. 1–5. [CrossRef]

108. Bozkurttas, M.; Mittal, R.; Dong, H.; Lauder, G.V.; Madden, P. Low-dimensional models and performance scaling of a highly deformable fish pectoral fin. *J. Fluid Mech.* **2009**, *631*, 311–342. [CrossRef]

109. Bozkurttas, M.; Tangorra, J.; Lauder, G.; Mittal, R. Understanding the hydrodynamics of swimming: From fish fins to flexible propulsors for autonomous underwater vehicles. *Adv. Sci. Technol.* **2008**, *58*, 193–202. [CrossRef]

110. Georgiades, C.; Nahon, M.; Buehler, M. Simulation of an underwater hexapod robot. *Ocean. Eng.* **2009**, *36*, 39–47. [CrossRef]

111. Long, J.H., Jr.; Schumacher, J.; Livingston, N.; Kemp, M. Four flippers or two? Tetrapodal swimming with an aquatic robot. *Bioinspiration Biomim.* **2006**, *1*, 20–29. [CrossRef]

112. Sitorus, P.E.; Nazaruddin, Y.Y.; Leksono, E.; Budiyono, A. Design and implementation of paired pectoral fins locomotion of labriform fish applied to a fish robot. *J. Bionic Eng.* **2009**, *6*, 37–45. [CrossRef]

113. Cai, Y.; Bi, S.; Zheng, L. Design and experiments of a robotic fish imitating cow-nosed ray. *J. Bionic Eng.* **2010**, *7*, 120–126. [CrossRef]

114. Punning, A.; Anton, M.; Kruusmaa, M.; Aabloo, A. A biologically inspired ray-like underwater robot with electroactive polymer pectoral fins. In Proceedings of the IEEE Conference on Mechatronics and Robotics, Aachen, Germany, 13–15 September 2004; pp. 241–245.

115. Chen, Z.; Um, T.I.; Bart-Smith, H. Ionic polymer-metal composite enabled robotic manta ray. *Electroact. Polym. Actuators Devices (EAPAD)* **2011**, *7976*, 797637. [CrossRef]

116. Clarck, R.P.; Smits, A.J. Thrust production and wake structure of a batoid-inspired oscillating fin. *J. Fluid Mech.* **2006**, *562*, 415–429. [CrossRef]

117. Low, K.H. Locomotion simulation and system integration of robotic fish with modular undulating fin. *Int. J. Simul.* **2008**, *7*, 64–77.

118. Zhang, Y.H.; Song, Y.; Yang, J.; Low, K.H. Numerical and experimental research on modular oscillating fin. *J. Bionic Eng.* **2008**, *5*, 13–23. [CrossRef]

119. Zhang, Y.H.; He, J.H. Research on influence on fin ray motion pattern on the propulsion of bionic undulating fins. *Chin. J. Eng. Des.* **2017**, *24*, 89–99. [CrossRef]

120. Low, K.H.; Willy, A. Biomimetic motion planning of an undulating robotic fish fin. *JVC/J. Vib. Control* **2006**, *12*, 1337–1359. [CrossRef]

121. Low, K.H. Design, development and locomotion control of bio-fish robot with undulating anal fins. *Int. J. Robot. Autom.* **2007**, *22*, 88–99. [CrossRef]

122. Low, K.H. Maneuvering of biomimetic fish by integrating a buoyancy body with modular undulating fins. *Int. J. Hum. Robot.* **2007**, *4*, 671–695. [CrossRef]

123. Hu, T.; Shen, L.; Low, K.H. Bionic asymmetry: From amiiform fish to undulating robotic fins. *Chin. Sci. Bull.* **2009**, *54*, 562–568. [CrossRef]

124. Low, K.H. Modelling and parametric study of modular undulating fin rays for fish robots. *Mech. Mach. Theory* **2009**, *44*, 615–632. [CrossRef]

125. Epstein, M.; Colgate, J.E.; Maciver, M.A. Generating thrust with a biologically-inspired robotic ribbon fin. In Proceedings of the 2006 IEEE/RSJ International Conference on Intelligent Robots and Systems, Beijing, China, 9–15 October 2006; pp. 2412–2417. [CrossRef]

126. MacIver, M.A.; Sharabash, N.M.; Nelson, M.E. Prey-capture behavior in gymnotid electric fish: Motion analysis and effects of water conductivity. *J. Exp. Biol.* **2001**, *204*, 543–557.

127. MacIver, M.A.; Fontaine, E.; Burdick, J.W. Designing future underwater vehicles: Principles and mechanisms of the weakly electric fish. *IEEE J. Ocean. Eng.* **2004**, *29*, 651–659. [CrossRef]

128. Siahmansouri, M.; Ghanbari, S.; Fakhrabadi, M.M.S. Design, implementation and control of a fish robot with undulating fins. *Int. J. Adv. Robot. Syst.* **2011**, *8*, 61–69. [CrossRef]

129. Conte, J.; Modarres-Sadeghi, Y.; Watts, M.N.; Hover, F.S.; Triantafyllou, M.S. A fast-starting mechanical fish that accelerates at 40 m s^{-2}. *Bioinspiration Biomim.* **2020**, *5*, 035004. [CrossRef] [PubMed]

130. Epps, B.P.; Techet, A.H. Impulse generated during unsteady maneuvering of swimming fish. *Exp. Fluids* **2007**, *43*, 691–700. [CrossRef]

131. Dabiri, J.O. Optimal vortex formation as a unifying principle in biological propulsion. *Annu. Rev. Fluid Mech.* **2009**, *41*, 17–33. [CrossRef]

132. Gharib, M.; Rambod, E.; Shariff, K. A universal time scale for vortex ring formation. *J. Fluid Mech.* **1998**, *360*, 121–140. [CrossRef]

133. Krueger, P.S.; Gharib, M. The significance of vortex ring formation to the impulse and thrust of a starting jet. *Phys. Fluids* **2003**, *15*, 1271–1281. [CrossRef]

134. Krueger, P.S. An over-pressure correction to the slug model for vortex ring circulation. *J. Fluid Mech.* **2005**, *545*, 427–443. [CrossRef]

135. Krueger, P.S. Measurement of propulsive power and evaluation of propulsive performance from the wake of a self-propelled vehicle. *Bioinspiration Biomim.* **2006**, *1*, S49. [CrossRef]

136. Ruiz, L.A.; Whittlesey, R.W.; Dabiri, J.O. Vortex-enhanced propulsion. *J. Fluid Mech.* **2011**, *668*, 5–32. [CrossRef]

137. Guo, S.; Shi, L.; Ye, X.; Li, L. A new jellyfish type of underwater microrobot. In Proceedings of the International Conference on Mechatronics and Automation (ICMA 2007), Harbin, China, 5–8 August 2007; pp. 509–514. [CrossRef]

138. Yang, Y.; Ye, X.; Guo, S. A new type of jellyfish-like microrobot. In Proceedings of the IEEE International Conference on Integration Technology (ICIT'07), Shenzhen, China, 20–24 March 2007; pp. 673–678. [CrossRef]

139. Shi, L.; Guo, S.; Asaka, K. A novel jellyfish-like biomimetic microrobot. In Proceedings of the IEEE/ICME International Conference on Complex Medical Engineering (CME), Gold Coast, Australia, 13–15 July 2010; pp. 277–281. [CrossRef]

140. Yeom, S.W.; Oh, I.K. A biomimetic jellyfish robot based on ionic polymer metal composite actuators. *Smart Mater. Struct.* **2009**, *18*, 085002. [CrossRef]

141. Villanueva, A.; Smith, C.; Priya, S. A biomimetic robotic jellyfish (Robojelly) actuated by shape memory alloy composite actuators. *Bioinspiration Biomim.* **2011**, *6*, 036004. [CrossRef] [PubMed]

142. Najem, J.; Sarles, S.A.; Akle, B.; Leo, D.J. Biomimetic jellyfish-inspired underwater vehicle actuated by ionic polymer metal composite actuators. *Smart Mater. Struct.* **2012**, *21*, 094026. [CrossRef]

143. Krieg, M.; Mohseni, K. Thrust characterization of a bioinspired vortex ring thruster for locomotion of underwater robots. *IEEE J. Ocean. Eng.* **2008**, *33*, 123–132. [CrossRef]

144. Krieg, M.; Mohseni, K. Dynamic modeling and control of biologically inspired vortex ring thrusters for underwater robot locomotion. *IEEE Trans. Robot.* **2010**, *26*, 542–554. [CrossRef]

145. Serchi, F.G.; Arienti, A.; Laschi, C. A biomimetic, swimming soft robot inspired by the Octopus vulgaris. *Lect. Notes Comput. Sci.* **2012**, *7375*, 349–351. [CrossRef]

146. Serchi, F.G.; Arienti, A.; Laschi, C. Biomimetic Vortex Propulsion: Toward the New Paradigm of Soft Unmanned Underwater Vehicles. *IEEE/ASME Trans. Mechatron.* **2013**, *18*, 484–493. [CrossRef]

147. Van Buren, T.; Floryan, D.; Brunner, D.; Senturk, U.; Smits, A.J. Impact of trailing edge shape on the wake and propulsive performance of pitching panels. *Phys. Rev. Fluids* **2017**, *2*, 014702. [CrossRef]

148. Shen, L.; Zhang, X.; Yue, D.K.P. Turbulent flow over a flexible wall undergoing a streamwise travelling wave motion. *J. Fluid Mech.* **2003**, *484*, 197–221. [CrossRef]

149. Liu, H.; Kawachi, K. A numerical study of undulatory swimming. *J. Comput. Phys.* **1999**, *155*, 223–247. [CrossRef]

150. Huera-Huarte, F.J. Propulsión acuática bio-inspirada basada en aleteo: Revisión y últimos avances. *DYNA Ingeniería e Industria* **2016**, *91*, 560–563. [CrossRef]

151. Gazzola, M.; Argentina, M.; Mahadevan, L. Scaling macroscopic aquatic locomotion. *Nat. Phys.* **2014**, *10*, 758–761. [CrossRef]

152. Taylor, G.K.; Nuds, R.L.; Thomas, A.L.R. Flying and swimming animals cruise at a Strouhal number tuned for high power efficiency. *Nature* **2003**, *425*, 707–711. [CrossRef] [PubMed]

153. Rohr, J.; Fish, F. Strouhal numbers and optimization of swimming by odontocete cetaceans. *J. Exp. Biol.* **2004**, *207*, 1633–1642. [CrossRef] [PubMed]

154. Triantafyllou, G.S.; Triantafyllou, M.S.; Grosengaugh, M.A. Optimal thrust development in oscillating foils with application to fish propulsion. *J. Fluids Struct.* **1993**, *7*, 205–224. [CrossRef]

155. Floch, F.; Phoemsatphawee, S.; Laurens, J.M.; Leroux, J.B. Porpoising foil as a propulsion system. *Ocean. Eng.* **2012**, *39*, 53–61. [CrossRef]

156. Katz, J.; Weihs, D. Hydrodynamic propulsion by large amplitude oscillations of an airfoil with chordwise flexibility. *J. Fluid Mech.* **1978**, *88*, 485–497. [CrossRef]

157. Jones, K.D.; Lai, J.C.S.; Tuncer, I.H.; Platzer, M.F. Computational and experimental investigation of flapping-foil propulsion. In Proceedings of the 1st International Symposium on Aqua Bio-Mechanisms/International Seminar on Aqua Bio-Mechanisms, Tokai University Pacific Center, Honolulu, HI, USA, 27–30 August 2000.

158. Lan, C.E. The unsteady quasi-vortex-lattice method with applications to animal propulsion. *J. Fluid Mech.* **1979**, *93*, 747–765. [CrossRef]

159. Isogai, K.; Shinmoto, Y.; Watanabe, Y. Effects of dynamic stall on propulsive efficiency and thrust of flapping airfoil. *AIAA J.* **1999**, *37*, 1145–1151. [CrossRef]

160. Triantalyllou, M.S.; Triantafillou, G.S.; Yue, D.K.P. Hydrodynamics of fishlike swimming. *Annu. Rev. Fluid Mech.* **2000**, *32*, 33–53. [CrossRef]

161. Lu, X.Y.; Yin, Z.X. Propulsive performance of a fish-like travelling wavy wall. *Acta Mech.* **2005**, *175*, 197–215. [CrossRef]

162. Blake, R.W. The mechanics of labriform locomotion II. An analysis of the recovery stroke and the overall fin-beat cycle propulsive efficiency in the alglefish. *J. Exp. Biol.* **1980**, *85*, 337–342.

163. Mattheijssens, J.; Marcel, J.P.; Bosschaerts, W.; Lefeber, D. Oscillating foils for ship propulsion. In Proceedings of the 9th National Congress on Theoretical and Applied Mechanics, Brussels, Belgium, 9–11 May 2012.

164. Kim, J.Y.; Ghajar, A.J.; Tang, C.; Fouth, G.L. Comparison of near-wall treatment methods for high Reynolds number backward-facing step flow. *Int. J. Comput. Fluid Dyn.* **2005**, *19*, 493–500. [CrossRef]

165. Tytell, E.D.; Hsu, C.Y.; Williams, T.L.; Cohen, A.H.; Fauci, L.J. Interactions between internal forces, body stiffness, and fluid environment in a neuromechanical model of lamprey swimming. *Proc. Natl. Acad. Sci. USA* **2010**, *107*, 19832–19837. [CrossRef]

166. Tytell, E.D.; Borazjani, I.; Sotiropoulos, F.; Baker, T.V.; Anderson, E.J.; Lauder, G.V. Disentangling the functional roles of morphology and motion in the swimming of fish. *Integr. Comp. Biol.* **2010**, *50*, 1140–1154. [CrossRef]

167. Bhalla, A.P.S.; Griffith, B.E.; Patankar, N.A. A forced damped oscillation framework for undulatory swimming provides new insights into how propulsion arises in active and passive swimming. *PLoS Comput. Biol.* **2013**, *9*, e1003097. [CrossRef]

168. Cherukat, P.; Na, Y.; Hanratty, T.J.; McLaughlin, J.B. Direct numerical simulation of a fully developed turbulent flow over a wavy wall. *Theor. Comput. Fluid Dyn.* **1998**, *11*, 109–134. [CrossRef]

169. Maass, C.; Schumann, U. *Numerical Simulation of Turbulent Flow over a Wavy Boundary*; Fluid Mechanics and Its Applications: Dordrecht, the Netherlands, 1994; pp. 287–297.

170. You, D.; Wang, M.; Mittal, R.; Moin, P. Large-Eddy simulations of longitudinal vortices embedded in a turbulent boundary layer. *AIAA J.* **2006**, *44*, 3032–3039. [CrossRef]

171. Hasse, C.; Sohm, V.; Wetzel, M. Hybrid URANS/LES turbulence simulation of vortex shedding behind a triangular flameholder. *Flow Turbul. Combust.* **2009**, *83*, 1–20. [CrossRef]

172. Balaras, E. Modeling complex boundaries using an external force field on fixed Cartesian grids in large-eddy simulations. *Comput. Fluids* **2004**, *33*, 375–404. [CrossRef]

173. Fauci, L.; Peskin, C.S. A computational model of aquatic animal locomotion. *J. Comput. Phys.* **1988**, *77*, 85–108. [CrossRef]

174. Van Rees, W.M.; Gazzola, M.; Koumoutsakos, P. Optimal shapes for anguilliform swimmers at intermediate Reynolds numbers. *J. Fluid Mech.* **2013**, *722*, R3. [CrossRef]

175. Tytell, E.D.; Leftwich, M.C.; Hsu, C.Y.; Griffith, B.E.; Cohen, A.H.; Smits, A.J.; Hamlet, C.; Fauci, L.J. Role of body stiffness in undulatory swimming: Insights from robotic and computational models. *Phys. Rev. Fluids* **2016**, *1*, 073202. [CrossRef]

176. Griffith, B.E.; Hornung, R.D.; McQueen, D.M.; Peskin, C.S. An adaptive, formally second order accurate version of the immersed boundary method. *J. Comput. Phys.* **2017**, *223*, 10–49. [CrossRef]

177. Griffith, B.E. An accurate and efficient method for the incompressible Navier–Stokes equations using the projection method as a preconditioner. *J. Comput. Phys.* **2009**, *228*, 7565–7595. [CrossRef]

178. Akhtar, I.; Mittal, R.; Lauder, G.V.; Drucker, E. Hydrodynamics of a biologically inspired tandem flapping foil configuration. *Theor. Comput. Fluid Dyn.* **2007**, *21*, 155–170. [CrossRef]

179. Gazzola, M.; Chatelain, P.; van Rees, W.M.; Koumoutsakos, P. Simulations of single and multiple swimmers with non-divergence free deforming geometries. *J. Comput. Phys.* **2011**, *230*, 7093–7114. [CrossRef]

180. Borazjani, I.; Sotiropoulos, F. Numerical investigation of the hydrodynamics of carangiform swimming in the transitional and inertial flow regimes. *J. Exp. Biol.* **2008**, *211*, 1541–1558. [CrossRef]

181. Dong, H.; Bozkurttas, M.; Mittal, R.; Madden, P.; Lauder, G.V. Computational modelling and analysis of the hydrodynamics of a highly deformable fish pectoral fin. *J. Fluid Mech.* **2010**, *645*, 345–373. [CrossRef]

182. Borazjani, I.; Sotiropoulos, F.; Tytell, E.D.; Lauder, G.V. Hydrodynamics of the bluegill sunfish c-start escape response: Three-dimensional simulations and comparison with experimental data. *J. Exp. Biol.* **2012**, *215*, 671–684. [CrossRef]

183. Mittal, R.; Iaccarino, G. Immersed boundary methods. *Annu. Rev. Fluid Mech.* **2005**, *37*, 239–261. [CrossRef]

184. Eldredge, J.D. Numerical simulatons of undulatory swimming at moderate Reynolds number. *Bioinspir. Biomim.* **2006**, *1*, S19–S24. [CrossRef] [PubMed]

185. Zhu, Q.; Yuming, L.; Yue, D.K.P. Dynamics of a three-dimensional oscillating foil near the free surface. *AIAA J.* **2006**, *44*, 2997–3009. [CrossRef]

186. De Silva, L.W.A.; Yamaguchi, H. Numerical study on active wave devouring propulsion. *J. Mar. Sci. Technol.* **2012**, *17*, 261–275. [CrossRef]

187. Filippas, E.S.; Belibassakis, K.A. Hydrodynamic analysis of flapping-foil thrusters operating beneath the free surface and in waves. *Eng. Anal. Bound. Elem.* **2014**, *41*, 47–59. [CrossRef]

188. Filippas, E.S.; Papadakis, G.P.; Belibassakis, K.A. Free-surface effects on the performance of flapping-foil thruster for augmenting ship propulsion in waves. *J. Mar. Sci. Eng.* **2020**, *8*, 357. [CrossRef]

189. Lauder, G.V.; Tytell, E.D. Hydrodynamics of undulatory propulsion. *Fish Biomech.* **2006**, *23*, 425–468. [CrossRef]

190. Babu, M.N.P.; Krishnankutty, P.; Mallikarjuna, J.M. Experimental study of flapping foil propulsion system for ships and underwater vehicles and PIV study of caudal fin propulsors. In Proceedings of the IEEE/OES Autonomous Underwater Vehicles, Oxford, MS, USA, 6–9 October 2014. [CrossRef]

191. Drucker, E.G.; Lauder, G.V. Locomotor forces on a swimming fish: Three-dimensional vortex wake dynamics quantified using digital particle image velocimetry. *J. Exp. Biol.* **1999**, *202*, 2393–2412. [PubMed]

192. Drucker, E.G.; Lauder, G.V. A hydrodynamic analysis of fish swimming speed: Wake structure and locomotor force in slow and fast labriform swimmers. *J. Exp. Biol.* **2000**, *203*, 2379–2393.

193. Drucker, E.G.; Lauder, G.V. Locomotor function of the dorsal fin in teleost fishes: Experimental analysis of wake forces in sunfish. *J. Exp. Biol.* **2001**, *204*, 2943–2958.

194. Videler, J.J.; Muller, U.K.; Stamhuis, E.J. Aquatic vertebrate locomotion: Wakes from body waves. *J. Exp. Biol.* **1999**, *202*, 2430–3423.

195. Videler, J.J.; Stamhuis, E.J.; Maijller, U.K.; van Duren, L.A. The scaling and structure of aquatic animal wakes. *Integr. Comp. Biol.* **2002**, *42*, 988–996. [CrossRef] [PubMed]

196. Muller, U.K.; Stamhuis, E.J.; Videler, J.J. Hydrodynamics of unsteady fish swimming and the effects of body size: Comparing the flow fields of fish larvae and adults. *J. Exp. Biol.* **2000**, *203*, 193–206. [PubMed]

197. Stamhuis, E.J.; Videler, J.J. Quantitative flow analysis around aquatic animals using laser sheet particle image velocimetry. *J. Exp. Biol.* **1995**, *198*, 283–294. [PubMed]

198. Wen, L.; Wang, T.M.; Wu, G.H.; Liang, J. Quantitative thrust efficiency of a self-propulsive robotic fish: Experimental method and hydrodynamic investigation. *IEEE/ASME Trans. Mechatron.* **2013**, *18*, 1027–1038. [CrossRef]

199. Wen, L.; Wang, T.M.; Wu, G.H.; Liang, J. Hydrodynamic investigation of a self-propulsive robotic fish based on a force-feedback control method. *Bioinspir. Biomim.* **2012**, *7*, 036012. [CrossRef] [PubMed]

200. Anderson, E.J.; McGillis, W.R.; Grosengaugh, M.A. The boundary layer of swimming fish. *J. Exp. Biol.* **2001**, *204*, 81–102.

201. Buckles, J.; Hanratty, T.J.; Adrian, R.J. Turbulent flow over a large-amplitude wavy surface. *J. Fluid Mech.* **1984**, *140*, 27–44. [CrossRef]

202. Kuzan, J.D.; Hanratty, T.J.; Adrian, R.J. Turbulent flows with incipient separation over solid waves. *Exp. Fluids* **1989**, *7*, 88–98. [CrossRef]

203. Hudson, J.D. The Effect of a Wavy Boundary on Turbulent Flow. Ph.D. Thesis, University of Illinoids Urbana, Champaign, IL, USA, 1993.

204. Hudson, J.D.; Dykhno, L.; Hanratty, T.J. Turbulence production in flow over a wavy wall. *Exp. Fluids* **1996**, *20*, 257–265. [CrossRef]